ACS OMEGA

http://pubs.acs.org/journal/acsodf

Article

Synchronous Monitoring of Cement Hydration and Polymer Film Formation Using ^{1}H-Time-Domain-NMR with T_2 Time-Weighted T_1 Time Evaluation: A Nondestructive Practicable Benchtop Method

Daniel Jansen,* Dominique Ectors, Xiangming Kong,* Christian Schmidtke, Florian Deschner, Joachim Pakusch, Ekkehard Jahns, and Jürgen Neubauer

Cite This: *ACS Omega* 2021, 6, 7499−7511

Read Online

ACCESS | Metrics & More | Article Recommendations

ABSTRACT: The interactions between latex and cement are still not completely understood. In this work, we would like to address the temporal changes in cement hardening and latex film formation. For this reason, the hydration process and the film formation were simultaneously monitored. This scientific issue is even more challenging as a nondestructive quantitative analysis of the film formation process is not available yet. Here, we report on simultaneous monitoring of the latex film formation and the phase development in cementitious systems via ^{1}H-time-domain-NMR for the first time. The obtained results were validated using classical analytical methods, such as in situ X-ray diffraction, X-ray fluorescence (Rietveld analysis), and confocal laser scanning microscopy.

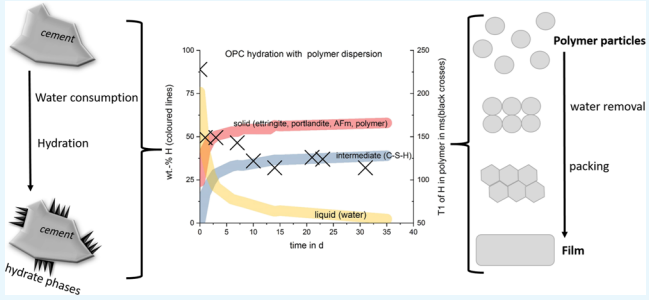

INTRODUCTION

Cement−polymer composites are of enormous interest in daily life and play an essential role in the dry mix mortar industry.[1] Polymer latex, which is also called polymer dispersion, can be applied as dispersions or dried redispersible powders and can significantly improve cement-based mortars, such as repair mortars, self-leveling underlayment, renders, tile adhesives, waterproofing membranes, and more. The use of polymer dispersions leads to a significant improvement in necessary properties such as adhesive strength, flexural strength, workability, or durability.[2,3]

The combination of cement and polymer latex leads to a very complex composite with a hardening process that can be divided into a chemical reaction (hydration of cement) and a physical coalescence of polymer particles caused by the interdiffusion of the polymer chains between the single polymer particles, which is known as film formation. During the composite/hybrid formation process, the cement consumes water, starts hydration, and builds new mineral phases. However, the latex particles might form a film because of concentration changes, ionic strength, and/or interactions with the hydration phases. Therefore, the dispersion as well as its film formation influences (retarding) the hydration process of the cement and vice versa. However, both reactions are highly temperature-dependent. Although the temperature mainly determines the reaction rate in hydration processes, film formation is a function of temperature. Below the so-called minimum film formation temperature (MFFT), there is no film formation, and the drying of a polymer dispersion results in an opaque powder or opaque solid. If the temperature is above the MFFT, the polymer chains can interdiffuse between the particles and a homogeneous transparent film results. The film formation of polymer particles is a well-observed phenomenon. The authors would like to refer to the relevant review literature.[4,5]

However, it is a scientific consensus that film formation takes place through different stages. Water evaporation causes a concentration of the polymer particles to occur. After the polymer particles have touched each other, they are deformed toward a hexagonal packing because of ongoing water evaporation and capillary pressure. Finally, the polymer chains interdiffuse and a more homogeneous structure (film) is formed.

There are many methods that have been used in order to examine film formation and obtain new insights into this process. Chen et al.[6] studied film formation at temperatures above the MFFT by means of synchrotron small-angle X-ray diffraction (XRD). They showed that during drying, the voids

Received: December 10, 2020
Accepted: February 4, 2021
Published: March 9, 2021

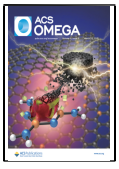

between the individual particles are first closed. The particles then form a face-centered cubic colloidal crystalline structure before the chains begin to interdiffuse.

The film formation process was also studied applying solid-state NMR spectroscopy.[7] It could be shown that the process of film formation strongly correlates to the drying of different types of water within the film. It seems that external water (between the particles) is removed differently than water in the ionic or nonionic groups of the polymer. Another technique to study film formation is inverse micro-Raman microscopy.[8] The method was applied successfully in order to examine the completeness of the film formation.

However, most examinations of film formation concentrate on pure dispersions/films. A method that is suitable for studying both cement hydration and polymer film formation in situ, artifact-free, and quantitatively has not been presented elsewhere. This scientific issue is even more challenging, as there is no nondestructive quantitative analysis of the film formation process available yet. Prior research addressed this topic qualitatively by using (cryo)-scanning electron microscopy (SEM) and transmission electron microscopy (TEM) analyses. Besides the problem of destructive analysis, these techniques require a lot of effort, provide only a snapshot of a complex process, and could lead to misinterpretations because of (ice) artifacts.[9]

Nowadays, ^{1}H-time-domain-NMR (^{1}H-TD-NMR) is a powerful tool in polymer science. Numerous scientific questions can now be answered by applying ^{1}H-TD-NMR. For an overview of the possibilities of the method, the authors refer to a recent published review.[10]

However, the idea of using ^{1}H-TD-NMR in order to study film formation was already discussed by Voogt et al.[11] It was shown that the drying rate has no impact on the hydrogen mobility during film formation and the hardening of the film. Nevertheless, it was discussed that the H mobilities of water and the mobile polymer phase decrease after most water evaporated.

If a polymer dispersion is added to the cement, as it is done for many applications, the whole analysis becomes more and more complex. Hence, the synchronous tracking of film formation and cement hydration using ^{1}H-TD-NMR is a formidable challenge.

During cement hydration, hydrate phases are formed,[12−16] which leads to the complication that in addition to water and polymer, even more H reservoirs occur. There is much literature on ^{1}H-TD-NMR during cement hydration available that discuss the challenges and opportunities of the method.[17−19] First, the method can be used reliably in order to follow the formation of hydrate phases during the hydration of cements.[20−22] Second, the method attracts attention because porosity[23−25] can be studied using ^{1}H-TD-NMR, which is of great interest for cement stones, inasmuch as porosity is a main factor affecting strength and durability.

The aim of the present work is to show the challenges and opportunities of ^{1}H-TD-NMR in order to follow both cement hydration and film formation. The fact that the presence of polymer particles has an impact on cement hydration[26−28] even further complicates the analytical work.

EXPERIMENTAL SECTION

Materials. The cement used in the study was white cement of the 52.5R type (OPC-type). The chemical and mineralogical compositions of the cement were studied using X-ray fluorescence and XRD (Rietveld analysis), respectively. The cement is composed of 65.7 wt % CaO, 21.4 wt % SiO_2, 4.1 wt % Al_2O_3, 0.3 wt % Fe_2O_3, 0.9 wt % MgO, 0.15 wt % Na_2O, 0.6 wt % K_2O, 3.8 wt % SO_3, and 0.2 wt % TiO_2. The quantitative phase analyses by Rietveld yielded 58 wt % alite, 23 wt % belite, 7.5 wt % C_3A cubic, 0.3 wt % gypsum, 3.8 wt % bassanite, 2.0% anhydrite, 2.8% calcite, 0.3 wt % arcanite, and 0.9 wt % syngenite.

Polymer dispersions were synthesized via emulsion polymerization. Two different copolymers with a variation in the monomer composition of *n*-butyl acrylate (BA) and styrene (St) were synthesized. The ratio between BA and St was adjusted, so that one polymer shows a T_g value of 58 °C, which will be called a hard polymer, and one polymer has T_g of −5 °C, which will be called a soft polymer.

In a standard semibatch emulsion polymerization, St, BA, and methacrylic acid were polymerized at 90 °C for 210 min using 0.55 pphm sodium persulfate. Stabilization is due to 0.1 pphm Disponil FES77 (Cognis) and 0.2 Lutensol AT18 (BASF SE) emulsifiers in the emulsion feed. Hard polymer uses 73/25/2 pphm St/BA/methacrylic acid. Soft polymer uses 36/62/2 pphm St/BA/methacrylic acid. The solid content is 40%.

The surface of both polymers was modified with anionic carboxylic groups in order to guarantee stability of the particles in dispersion, even after removing the aqueous phase. Both types of polymer particles show a comparable particle size (mean diameter around 300 nm), and both show a high negative charge at a pH of 12 (−120 ueq/g for hard polymer and −162 ueq/g for soft polymer). Both polymer dispersions were cleaned by dialysis before being used in the experiments. This was done in order to simplify the starting point of examinations, inasmuch as oligomers, residual monomers, and emulsifiers are removed by dialysis and will not produce a signal in the ^{1}H-TD-NMR measurements. Dialysis was done using a semipermeable membrane with a pore size of 24 Å (Visking dialysis tubing 12−14,000 Da, 0.04 mm wall thickness, 1.5 in. diameter, Medicell Membranes Ltd., Greenwich, UK). Dialysis of 300 g dispersion, diluted by half with water, in 5 L of desalinated water was performed until the conductivity of the dialysate dropped from around 1200 μS/cm to below 15 mS/cm, which needs 3−5 days with a daily exchange of the fully desalinated water (10 μS/cm). The stability of the cleaned dispersion in a high ionic solution was confirmed and is guaranteed because of the high ionic charge on the surface of the particle because of the carboxylic groups.

Pure alite was synthesized using $CaCO_3$, Al_2O_3, and SiO_2 from Alfa Aesar. Al_2O_3 was used to stabilize the monoclinic (M3) alite structure. After weighing and homogenization, the powder was sintered two times at 1450 °C for 4 h. Between the two sintering steps, the powder was homogenized. Phase purity was checked with XRD and Rietveld refinement.

All studies were performed with demineralized water at a temperature of 23 °C and a water/cement ratio of 0.5. The amount of polymer used was 10 wt % with respect to cement. The type of polymer used in the experiment (hard or soft polymer) is indicated in the figures.

Instrumentation. In situ XRD was performed with a Bruker D8 diffractometer equipped with a LynxEye detector. The respective mixture was mixed properly with a spatula and then placed into a special sample holder that allows cooling and heating of the system.[29] XRD patterns were recorded at an interval of 10 min during hydration. Each pattern was analyzed

https://dx.doi.org/10.1021/acsomega.0c06010
ACS Omega 2021, 6, 7499−7511

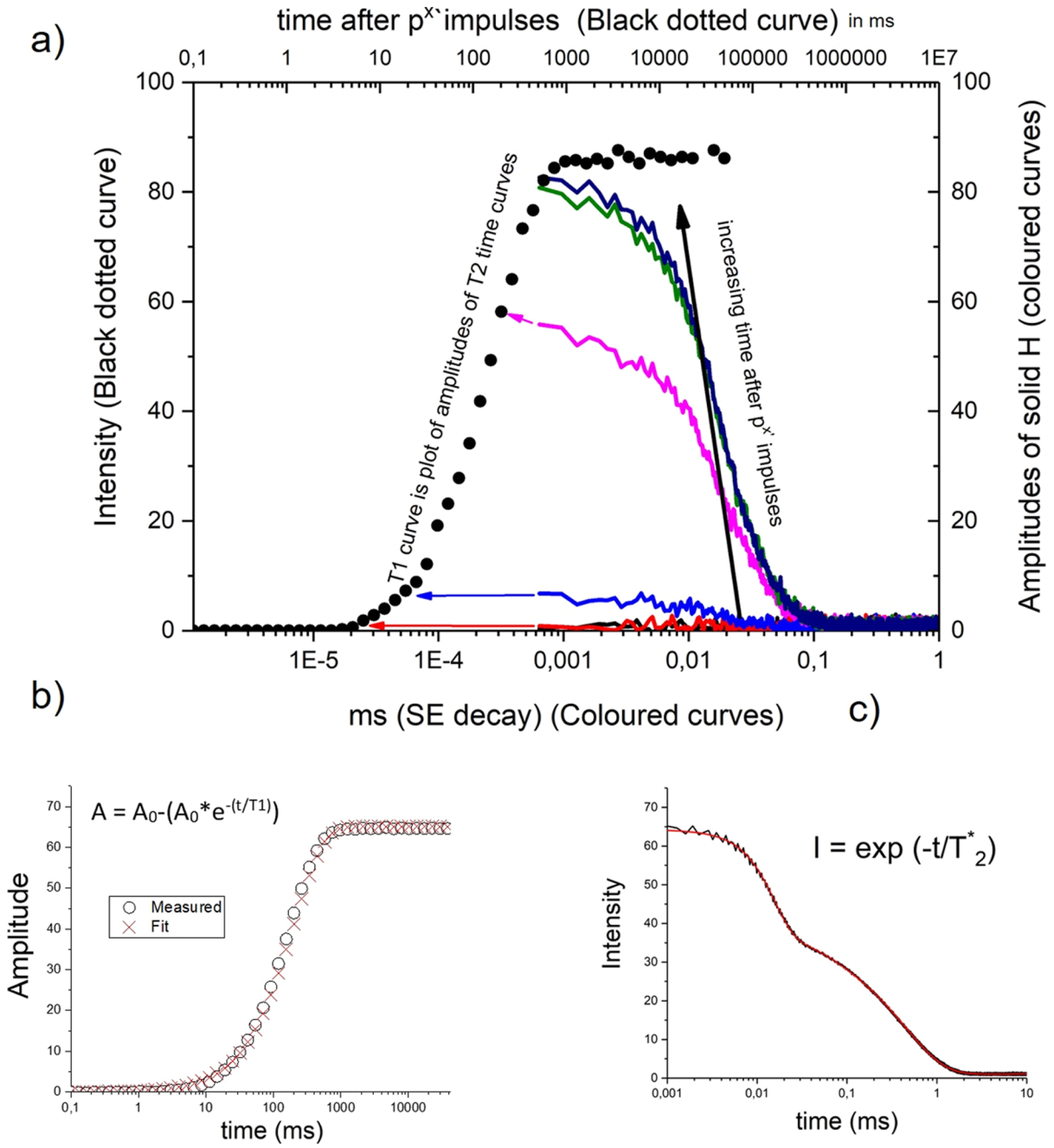

Figure 1. (a) T_2 and T_1 time curves, as obtained from the measurements of a sample with one H reservoir (here, a dried film from a cleaned polymer dispersion). (b) T_1 time curve of a dry polymer film of the soft polymer including the fitted curve. (c) T_2 time curve of a polymer latex from a soft polymer with reservoirs for solid and liquid including the fitted curve.

quantitatively, applying the Rietveld method[30] combined with an external standard procedure.[31−33] This procedure allows an absolute quantitative evaluation of each crystalline phase by considering the amorphous content, such as water and polymer particles. Rietveld analysis requires structural data from each crystalline phase. A complete list of all phases used in the present study and the corresponding reference to all original structural data can be found in a detailed study of the hydration of the cement that was also used in the present study.[20]

^{1}H-TD-NMR experiments were performed using a benchtop Bruker minispec mq 20 device. The device is equipped with a temperature-controlled probe head that allows the equilibration of the sample at 23 °C. T_2 and T_1 time curves were recorded.

The T_1 time curves are all saturation recovery curves. First, all coherence among the spins was destroyed, so that the bulk magnetization was set to zero. To this end, 10,000 px' pulses were applied in order to obtain a T_2 time curve that shows no intensity (see Figure 1a; red and black curves). At defined times, after the destruction of the coherence, solid-echo (SE) curves[34] were recorded, as can be seen in Figure 1a. The colored curves show examples after defined times, after the initial px' pulses. The increasing intensity of the SE curves shows the recovery of magnetization with time. The plot of the respective intensities of the single SE curves (50 single

https://dx.doi.org/10.1021/acsomega.0c06010
ACS Omega 2021, 6, 7499−7511

measurements for each T_1 time curve) against the recovery time after the px' pulses yields the T_1 time curve, as can be seen in Figure 1a (black dotted line). The SE pulse sequence was chosen because it allows the quantification of very fast-relaxing T_2 components, which are, for example, hydrogen in hydrate phases such as ettringite, portlandite, AFm,[17−21] and, as it will be shown later, hydrogen in the polymer particles as well (see also ref 10).

Examples of the T_1 time curves (saturation recovery) and the T_2 time curves (SE) are visible in Figure 1b,c. Figure 1b shows an example of a T_1 time curve with one reservoir (in this case, only H in the polymer film), whereas Figure 1c shows an example of a SE curve of a polymer dispersion showing hydrogen bound in water and hydrogen bound in a polymer. Both figures show the recorded curve and the fitted curve (in red). The respective mathematical equations for the fitting procedure are stated in the respective figures. The SE delay for the solid-echo measurements was 0.0055 ms, and the SE window chosen was 10 ms.

For the deconvolution of all the hydrogen signals accumulated in the solid part of the T_2 time curves, a special evaluation method was used. By applying the so-called T_2 time-weighted T_1 time evaluation, only specific signals of the T_2 time curve are plotted as the T_1 time curve, which in turn can then be evaluated in qualitative and quantitative terms. This in turn allows us to distinguish between different hydrogen reservoirs in the solid fraction. Since already the T_2 time curves are of high interest and results of our experiments, the whole procedure will be also explained with more figures in the Results and Discussion part (deconvolution of the recorded H reservoirs...).

The film formation behavior of latex particles was additionally characterized by confocal laser scanning microscopy (CLSM) using a Leica SP8 with a water immersion lens (63×, 1.2 NA). This technique allows optical sectioning, both horizontally and vertically, with a lateral resolution of >200 nm and a vertical resolution of >400 nm. The imaging contrast can be based on fluorescence or reflection/scattering (refractive index differences). In order to enhance the fluorescence contrast of the hydrophobic compartments of the latex, the lipophilic dye Nile red was used as the staining agent. The air voids as well as inorganic materials (hydration phases and fillers) appear dark under these conditions, showing nearly no (auto-) fluorescence even under the highest laser intensities. For sample preparation, the hardened latex-modified mortar layer was broken and incubated overnight (∼24 h) in water with 50 ppm Nile red (by weight) to allow sufficient migration of the hydrophobic dye into the polymer latexes. Afterward, CLSM imaging of the cross section of the fracture edge was performed using an excitation wavelength of 561 nm. The fluorescence was detected at a wavelength of 570−700 nm. Thus, all organic hydrophobic regions appear bright [fluorescence intensity depicted as a glow scale lookup table, i.e., low (dark) to high intensity (yellow-white)]."

RESULTS AND DISCUSSION

Deconvolution of the Recorded H Reservoirs and Assignment to H-Containing Phases. One of the major tasks when working with polymer−cement composites and ^{1}H-TD-NMR is the deconvolution of the different signals from the hydrogen environments in the sample and the assignment of the reservoirs to the correct physical phases. As is well known, several hydrate phases are formed during the hydration of an ordinary Portland cement (OPC)-type cement. Figure 2 shows the results from in situ XRD of the cement used in the present

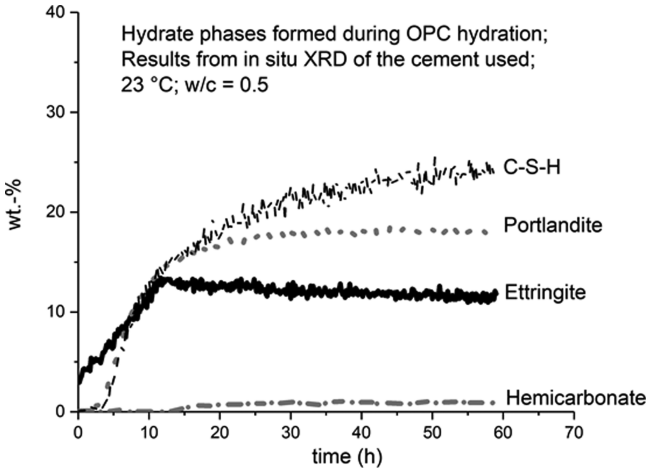

Figure 2. Evolution of the H-containing hydrate phases during OPC hydration determined by XRD analysis.

study. The results presented show the formation of the hydrate phases for the system without polymers. However, the hydrate phases formed are the same if the polymers used in our study are present during hydration, although the hydration process might be slowed down significantly.[26,27] As can be seen from Figure 2, the hydrate phases formed are calcium−silicate−hydrate (C−S−H), portlandite, ettringite, and AFm phase, which is hemicarbonate in our case. It can also be seen that the kinetics of the phase formation are quite complex. For a detailed discussion of the origin of the kinetics of cement hydration, the authors refer to other literature.[13,20,35,36]

However, it is known that especially hydrogen bound in the crystalline phases of ettringite, portlandite, and hemicarbonate shows a very fast relaxation time. This can be seen in Figure 3.

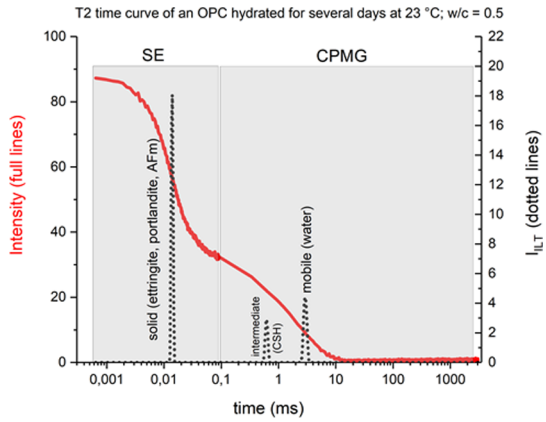

Figure 3. T_2 time curve of a hydrated OPC showing the different reservoirs which can be obtained from T_2 time measurements.

Here, a typical relaxation curve is shown, which was obtained from a single SE-Carr−Purcell−Meiboom−Gill (CPMG) pulse sequence[37,38] experiment performed on the cement. With inverse Laplace transformation (ILT) and applying the framework from Provencher,[39] at least three reservoirs can be obtained.

https://dx.doi.org/10.1021/acsomega.0c06010
ACS Omega 2021, 6, 7499−7511

It can be seen that hydrogen bound in ettringite, portlandite, and AFm (in our case hemicarbonate) cannot be distinguished using a T_2 time experiment. The ILT results in one reservoir, which occurs at around 0.015 ms.[19,20] Between 0.1 and 1 ms, hydrogen in the gel pores and the semicrystalline C−S−H phase can be quantified, as can be seen in Figure 3. However, as a function of fitting parameters and regulation parameters, the C−S−H reservoir can also be separated into several reservoirs representing water in the C−S−H gel pores and hydrogen in interlayer water.[23,40] At longer relaxation times, hydrogen in free nonreacted water can be measured and quantified.

Figure 4 shows the SE curve of the dispersion with the soft polymer synthesized and cleaned for the present study (black curve). It can be seen that there are mainly two reservoirs for hydrogen in the sample. First, the reservoir at a very early time, which might be hydrogen bound in the polymer particles, and second, hydrogen that shows a decay at later times, namely at a time longer than 1 ms. In order to prove the assumption, the quantitatively same amount of dispersion that was measured and represented the black curve was dried until a transparent film was obtained. The red curve represents the decay curve from the SE experiment with the film. The reservoir at later points in time disappeared, and only the reservoir at earlier times is visible. Furthermore, the same amount of water that was present in the dispersion was weighed in a sample holder and measured. The blue curve represents the quantitative amount of water from the dispersion. It can be clearly seen that the black curve is a sum of the red curve and the blue curve. Thus, this leads to the conclusion that hydrogen in the polymer particles can be detected and measured at quite short relaxation times. The small differences in the relaxation time of hydrogen bound in pure water (blue curve) and hydrogen bound in the water molecules of the dispersion (black curve) seem to be caused by the confinement of the water molecules because of the presence of the soft polymer particles, most likely due to the surface charge of the polymer particles introduced by the carboxylic groups.

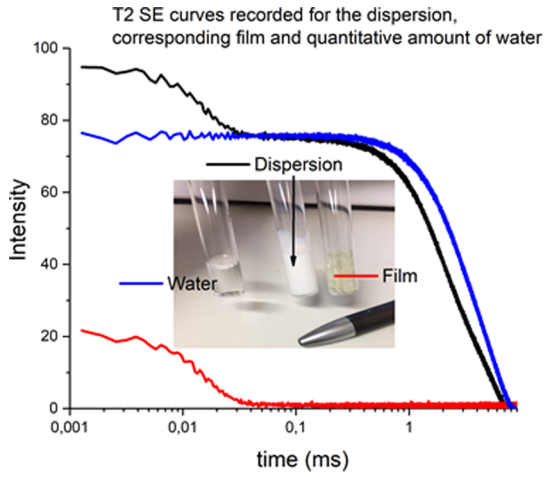

Figure 4. T_2 time curves for the dispersion, corresponding film, and quantitative amount of water corresponding to the dispersion (all experiments were performed using the soft polymer).

However, the performed experiments yield the following conclusions and challenges. Figure 5 shows the results from an in situ ^{1}H-TD-NMR experiment, involving the cement used with the soft polymer. The T_2 time is plotted against the hydration time. The intensity is given as a gray level. As discussed before, at least three reservoirs can be seen. The solid part at very early relaxation times comprises hydrogen bound in ettringite, portlandite, AFm, as well as hydrogen bound in the soft polymer added to the mixture. The intermediate phase comprises water associated with the C−S−H phase and the liquid reservoir comprises hydrogen in free water. However, it has to be concluded that this overlapping information rules out

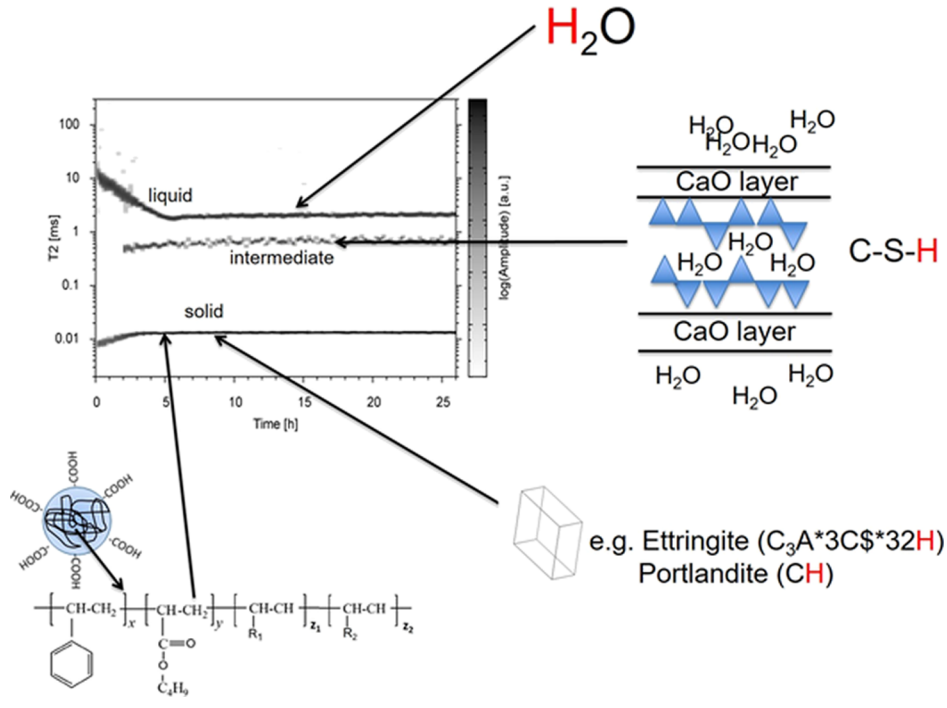

Figure 5. Assignment of the recorded reservoirs during T_2 time experiments. OPC used with the addition of the soft polymer.

https://dx.doi.org/10.1021/acsomega.0c06010
ACS Omega 2021, 6, 7499−7511

the possibility to gain an isolated signal for hydrogen in the polymer particle using T_2 time experiments.

Figure 6 shows the relation between T_1 and T_2 times to the molecular mobility of hydrogens. As discussed before, hydrogen in the hydrate phase crystals as well as in the polymer particles follows a very short T_2 time, as hydrogen is highly confined and its molecular mobility is very low. Water in gel pores and the interlayer water of the short crystalline C−S−H phase show medium T_2 times because of the less confinement and higher molecular mobility compared to hydrogen in the hydrate phase crystals.

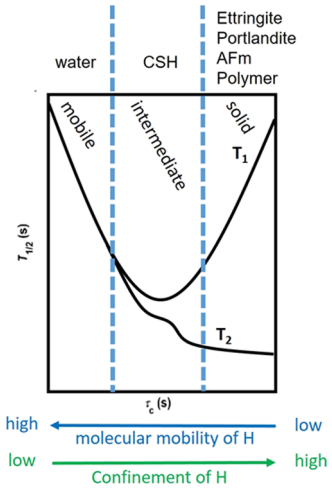

Figure 6. Evolution of T_1 time and T_2 time over the molecular mobility of hydrogen (own figure following figure from ref 42).

However, the reason why hydrogen in ettringite, portlandite, hemicarbonate, and polymer particles cannot be distinguished is also visible in Figure 6. As can be seen at very low molecular mobility, there is no further change in T_2 if there is a further confinement or freedom within the range of highly confined hydrogen. The T_2 evolution curve flattens at a high confinement. Hence, it is most likely to use T_1 time in order to distinguish the reservoirs at a highly confined level.[40,41] In addition to the discussed issues, there is one more reason why the T_1 time becomes the most interesting time for the present study. As mentioned in Introduction, it is the objective of this work to obtain a physical parameter that can be measured and correlated to the film formation of polymer particles during water consumption because of cement hydration in a cement−polymer−water mixture.

However, as it was shown that hydrogen in the polymer particles already shows a very high confinement, it is not conceivable that a further shift in T_2 time can be expected during film formation as the T_2 time does not change significantly at already highly confined hydrogen atoms. This can also be seen in Figure 4, where the solid hydrogen part of the dispersion (H in polymer particles) is found at equal T_2 times as hydrogen in the polymer film.

When looking at the change in T_1 time over molecular mobility in Figure 6, one can see that there is still a reasonable shift in T_1 time at low molecular mobilities. It is conceivable that there will be a signal shift in the T_1 time when polymer particles dry and coalesce during film formation.

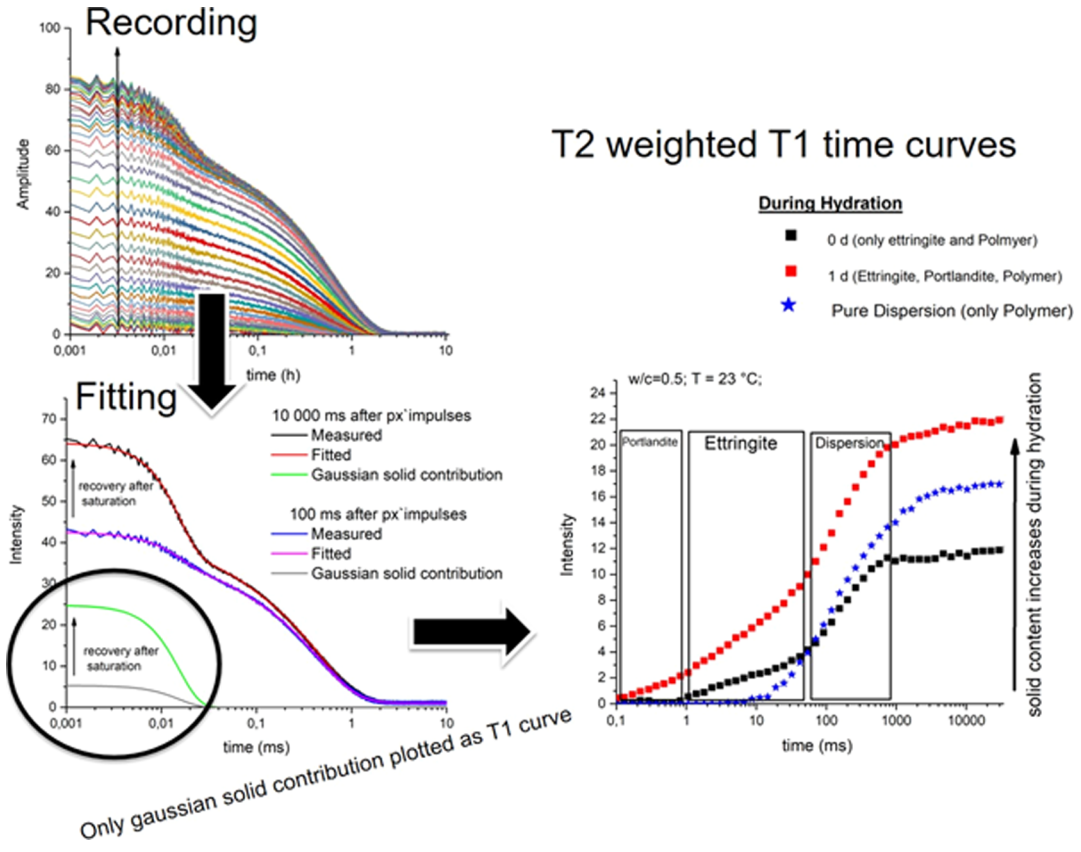

Figure 7. Explanation for the T_2-weighted T_1 time evaluation for the present study shown with the OPC used with the addition of 10 wt % of the soft polymer dispersion.

https://dx.doi.org/10.1021/acsomega.0c06010
ACS Omega 2021, 6, 7499−7511

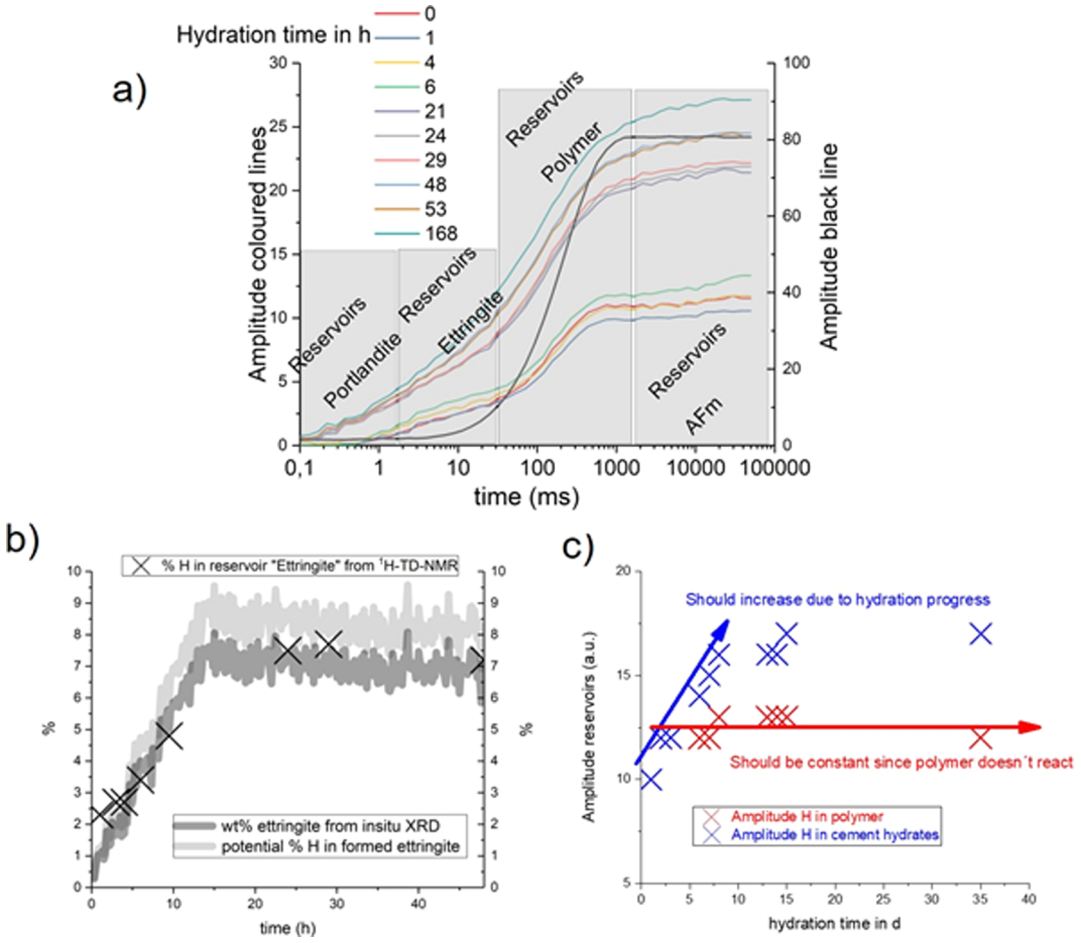

Figure 8. (a) Recorded curves over time of the OPC polymer mixture during hydration. (b) Comparison of the reservoir "ettringite" with the ettringite measured directly by in situ XRD. (c) Sum of the reservoir "hydrate phases" and reservoir "polymer" plotted quantitatively over time.

A final challenge arises when looking at Figure 6. As can be seen, it is possible that hydrogen with a high molecular mobility might have the same T_1 time as hydrogen with a low molecular mobility. This might cause a problem, as in our systems, highly confined hydrogen of ettringite, portlandite, polymer, and so forth appears next to less confined hydrogen from water. Consequently, there may be a signal overlap in the T_1 time that leads to measurement artifacts and distorts the evaluation of the T_1 times of our hydrogen reservoirs.

In order to bypass this problem, a T_2-weighted T_1 time evaluation approach was chosen and will be evaluated in our system. The procedure of this approach is explained in detail in Figure 7.

First, the saturation recovery T_1 time curves are recorded via 50 SE curves at defined times, after the destruction of the coherence among the spins. One example for all the curves can be seen in Figure 7. The longer the time after the destruction of the coherence, the more intensity is measured because of the recovery of the bulk magnetization. Second, each of the 50 curves is evaluated with an ILT, as can be seen in Figure 7 at the bottom left. Two examples are shown for SE curves after defined times, after the saturation impulses. After 100 ms, less intensity can be seen compared to that after 10,000 ms because of the fact that not all spins have already been recovered at 100 ms. The bottom left part of Figure 7 also shows the refinement of the curves and the contribution of the solid part to the fit of the curve (the highly confined part in the sample, which is hydrogen in the polymer and the crystalline hydrate phases). In order to avoid the T_1 time overlap of hydrogen in solids and water (as mentioned above) and to further distinguish the different reservoirs of the solid part, only the amplitude of the refined solid contribution is plotted as the T_1 time curve against the time after the coherence-destroying px' impulses, as can be seen in Figure 7 in the right part.

If the recorded T_1 time curves are plotted with respect to the elapsed hydration time, different reservoirs evolve. In Figure 7, on the right, it can be seen that the T_1 time curve of the prepared polymer film from the soft polymer without cement (blue stars) differs from the curve recorded directly after mixing the cement−water−polymer mixture. Besides the reservoir of the polymer, another reservoir occurs at around 10 ms (fitted curves will be discussed in detail later). As it is known and shown for the cement that ettringite is initially precipitated after mixing (see also Figure 2), it is most likely that the new reservoir can be assigned to hydrogen bound in ettringite. At later points in time, portlandite is formed and contributes to the solid reservoir that now becomes visible in the T_1 time curve at an early relaxation time (around 1 ms).

Figure 8a shows the T_2 time-weighted T_1 time curves during the hydration of the OPC used with 10 wt % of soft polymer after 0, 1, 4, 6, 21, 24, 29, 48, 53, and 168 h of hydration. As can be expected from Figure 2, the reservoir ettringite is visible from the beginning of hydration and increases over time. The reservoir portlandite is not visible within the first hours but

https://dx.doi.org/10.1021/acsomega.0c06010
ACS Omega 2021, 6, 7499−7511

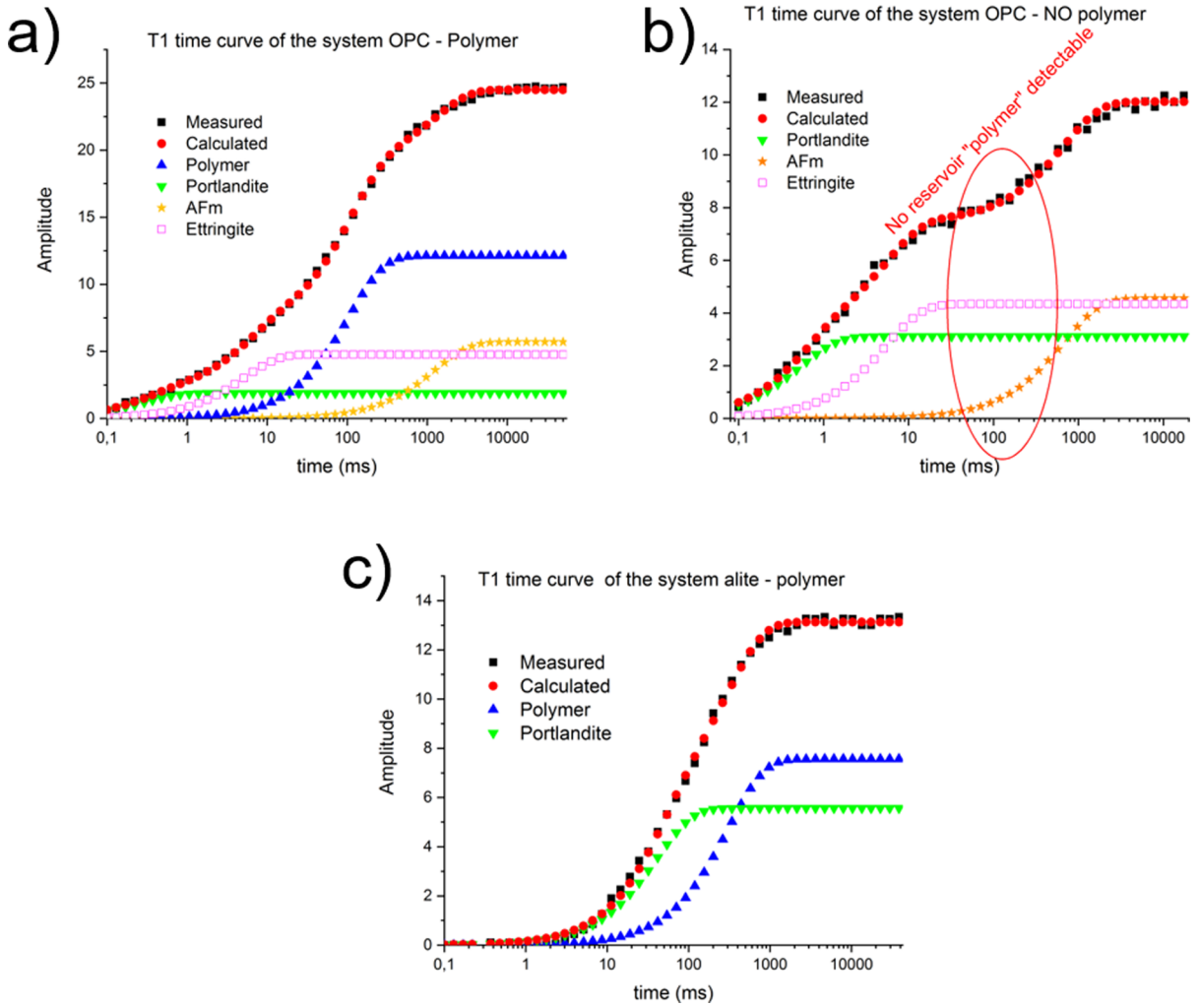

Figure 9. T_2 time-weighted T_1 time curves of (a) OPC−soft polymer system; (b) OPC system; and (c) alite−soft polymer system.

appears after several hours. Additionally, with regard to the curves during cement hydration, the T_1 time curve of the pure polymer film without cement is plotted in Figure 8a as the black curve. It can be seen that there is a reservoir visible in the cement−polymer paste, which can be assumed from the pure polymer experiment. At short hydration times, the T_1 time curves flatten at longer relaxation times (at around 10,000 ms), which is evidence that there is no further reservoir. However, after longer hydration times, one more reservoir is required in order to fit the curve at long relaxation times (also shown in Figure 9). It is most likely that a contribution from the subsequently formed AFm phase (in our case, hemicarbonate) appears here.

In order to further prove the correct assignment of the reservoirs, the following considerations were made. Figure 8b shows the evolution of the quantity (%of all hydrogen in the sample) of the reservoir which was assigned to the reservoir ettringite. This curve was compared to the wt % of ettringite formed that was measured by means of in situ XRD. The wt % from in situ XRD was also recalculated to the potential % hydrogen with respect to all hydrogen in the sample. It can be shown that the curves are in good agreement within the error of the methods (the error of the Rietveld method has to be estimated by ±1.5 wt % of ettringite). Especially, the very good agreement of the development of the curves over hydration time provides good evidence that the assignment of the reservoir is correct. Figure 8c shows the evolution of % H in all reservoirs that were assigned to the cement hydrate phases as well as the development of the reservoir that was assigned to hydrogen in the polymer particles. As the polymers are not consumed during the hydration process, it is most likely that the amplitude of the reservoir stays constant over the hydration time. The same consideration can be made for the hydrate phase, with the difference that hydrate phases grow during hydration, and hence the amplitude of the reservoirs should increase with time. As can be seen in Figure 8c, the considerations are in good agreement with the results from the experiments. The amplitude of the polymer reservoir stays constant over time, and the amplitude of the hydrate phase reservoirs increases with the hydration time.

Some more basic experiments were performed in order to prove the correct assignment of the reservoirs. Figure 9a shows a T_1 time curve of OPC used with 10% of the soft polymer after 2 days of hydration. The curve can be fitted well with four reservoirs that can be assigned to hydrogen in the polymer and the hydrate phases portlandite, ettringite, and AFm (hemicarbonate), which are all present in the sample at the point in time of the measurements, as can be seen from the XRD patterns (Figure 2). These findings are verified from Figure 9b that shows the curve of the cement without any addition of

https://dx.doi.org/10.1021/acsomega.0c06010
ACS Omega 2021, 6, 7499−7511

polymers at a comparable hydration time. It can be seen that a good fit can be achieved even without using a reservoir for hydrogen in the polymer at around 100 ms. The other reservoirs for ettringite, portlandite, and AFm have to be added in order to get a reasonable fit.

Following these considerations, a further experiment was performed using synthetic alite with the soft polymer. It is known from the literature that pure alite only forms portlandite and C−S−H. Hence, in our T_2-weighted T_1 time curve, there should only be two reservoirs, namely one for the portlandite and one for hydrogen in the soft polymer. No reservoirs for ettringite and AFm should be necessary. As can be seen in Figure 9c, there is a reasonable fit of the curve of pure alite with the polymer with only two reservoirs. However, the position of the reservoirs, especially portlandite, seems to differ a little bit from the position in the cement paste, which is most likely due to the different particle size distribution of the powders. Nevertheless, the number of theoretical and measured reservoirs is in very good agreement, and especially the assignment of the reservoir polymer seems to be reasonable because of the findings of all performed experiments.

Interpretation of the Signal Evolution of the T_1 Time of H in Polymer. The aim of the present study is to get an idea about how a synchronous tracking of cement hydration and film formation can be achieved. As shown above and in the literature, the SE-CPMG curves recorded during cement hydration can be evaluated quantitatively and plotted against time. As a result, one can get an idea about the hydration process of the cement. In Figure 10 the quantities of the different reservoirs are plotted. One can see that the reservoir for the hydrate phases increases over time (red curve for ettringite, portlandite, AFm, and blue for C−S−H) and that the reservoir for free water decreases because of the consumption of water during cement hydration.

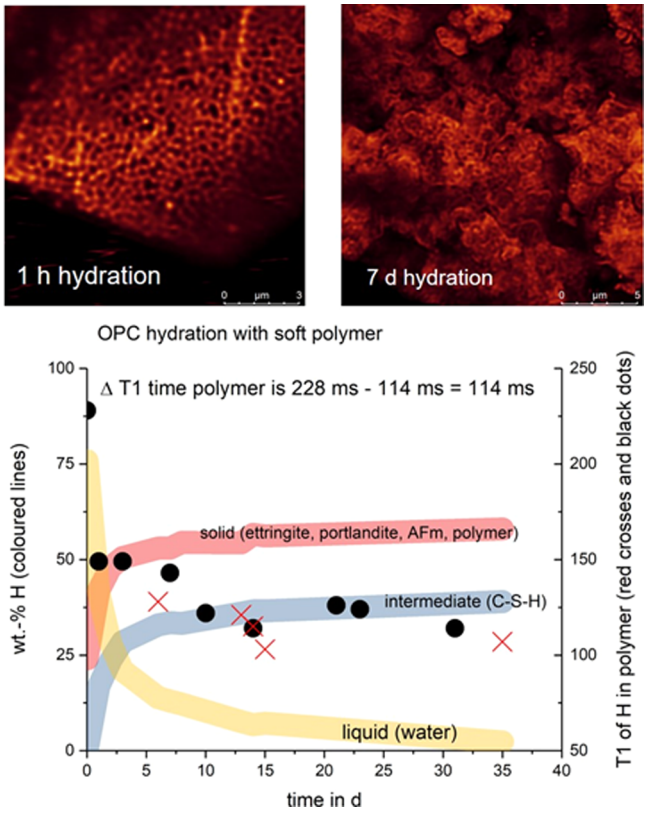

Figure 10. Top: Fluorescence microscopy images; Bottom: T_1 time of hydrogen in the soft polymer (two reproductions are shown as black dots and red crosses) and quantities of the reservoirs (hydrate phases and water) against hydration time.

In order to get an idea about film formation, it is not sufficient to plot the quantity of the reservoir of the polymer, as shown in Figure 8c, inasmuch as the polymer is not consumed, and the amount of hydrogen in the reservoir polymer will stay constant over the hydration time.

However, it is possible to plot the T_1 time for the reservoir polymer, as determined by fitting against the hydration time of the polymer−cement composite. As shown in Figure 10 (see black dots and red crosses for two reproductions), there is a shift in T_1 of hydrogen in the soft polymer particles during the hydration of the polymer−cement composite. The T_1 time at the beginning of hydration is around 228 ms and increases rapidly. From around 8 to 35 days, the T_1 time stays constant over time.

The question that arises from this observation is how this shift can be explained. Initial evidence is provided by the fluorescence microscopy measurements performed.

As can be seen in Figure 10, the single polymer particles can be visually separated after a short time of hydration. At later points in time, when the determined T_1 time of hydrogen in the polymer particles stays constant, there is no evidence of single polymer particles from fluorescence microscopy, and hence it has to be assumed that a homogeneous film is formed.

The best insights into the physical background of the T_1 time shift can be obtained from experiments with pure polymer dispersions. In the following case, the hard polymer dispersion was used in order to decouple drying and film formation. Figure 11 shows the T_1 time shift of hydrogen in the polymer particles during drying at defined temperatures. The results shown here are achieved with the hard polymer with a T_g value of 50 °C. Hence, the dispersion can be dried at room temperature, resulting in an opaque, dry powder, and no homogeneous transparent film can be observed. At higher temperatures, the material becomes transparent and homogeneous as a result of the coalescence of the polymer particles because of the interdiffusion of the polymer chains.

Hydrogen in the polymer particles in the dispersion shows a T_1 time of 634 ms. After drying at room temperature, hydrogen in the polymer particles shows a T_1 time of 384 ms. Further temperature treatment results in a more transparent solid at 50 °C and a very homogeneous film at 80 °C. The T_1 time shifts from 384 ms (room temperature) to 453 ms (50 °C) and 583 ms (80 °C).

The results obtained from the experiments can be explained as follows. Water is removed when the polymer dispersions dry. First, free water is removed, and then water in the polymer particles is removed. Figure 12 shows where water in the polymer particles can be assumed. The oxygen as well as the hydroxyl groups offer the potential for the accumulation of water molecules. If this water is removed, the T_1 time shifts to lower values that correspond to a gain in molecular mobility for the H atoms in the polymer particles (see Figure 6). This is more than reasonable because hydrogen from the polymer chains loses confinement by the release of water from the particles and the disappearance of hydrogen bound to the water molecules. Additionally, particles gain additional space if the water molecules are removed, resulting in more molecular mobility for hydrogen in the polymer chains.

https://dx.doi.org/10.1021/acsomega.0c06010
ACS Omega 2021, 6, 7499−7511

	Polymer Dispersion	Dried Polymer Particles	Homogeneous Film
T1 of hard polymer in ms	634	384	583
Confinement	Highest confinement	Lowest confinement	Medium confinement

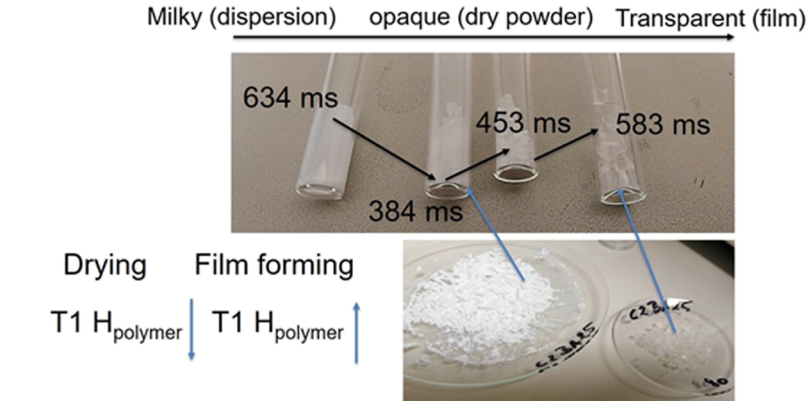

Figure 11. T_1 time shift during drying of the hard polymer dispersions at defined times and the corresponding T_1 time.

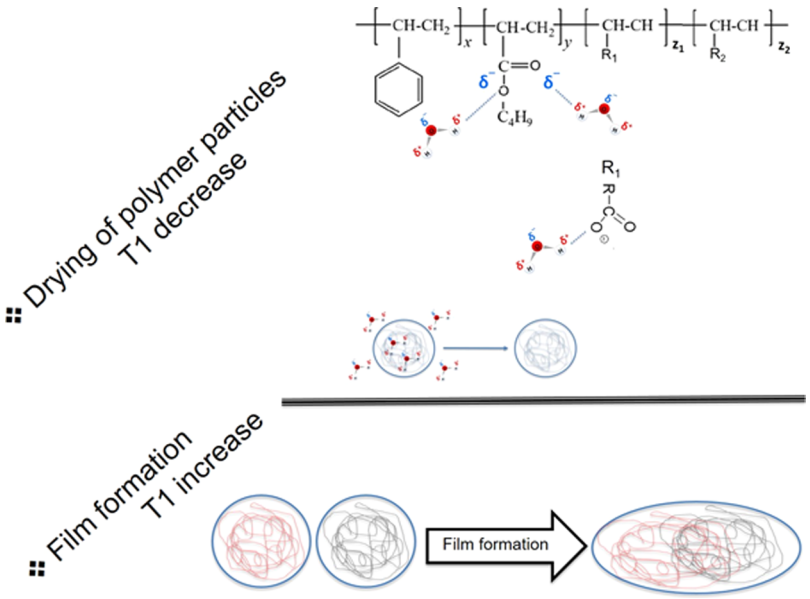

Figure 12. Schematic presentation of the mechanisms taking place during drying/film formation and the corresponding T_1 time shift.

In contrast to this, the coalescence of the polymer particles into a homogeneous, transparent film at higher temperatures causes a T_1 time shift to later T_1 times. This shift is caused by an increasing confinement of hydrogen in the particles or a less molecular mobility of hydrogen in the particles. This in turn can be explained by the interdiffusion of the polymer chains, as shown in Figure 12.

In the following, we explain these findings on a more molecular scale: as discussed by Voogt et al., the rigid (hard) fraction—in our case, the hydrophobic St compartments—with low hydrogen mobility does not have a strong interaction with water.[11] On a molecular level and because of the hydrophobic effect, these domains are arranged into structures that minimize their surfaces that are in contact with water. Thus, their mobility in water is reduced, and exposed regions are surrounded by highly ordered water molecules. After drying and before film formation, these hydrophobic parts gain more molecular mobility. When the temperature is increased above the MFFT, the polymer chains diffuse across the particle boundaries (coalescence) and penetrate through the thin layers of surfactants surrounding the latex particles.[7] As a consequence, the polymer chains occupy less space and are densely packed, whereby the molecular mobility of the polymeric hydrogens is reduced.

The soft polymer domains consist of hydrophilic acrylic moieties, serum, and surfactants. This part is swollen and plasticized by water.[7] During evaporation and further film formation, the soft part loses its hydrogen mobility.

However, it can be summarized that drying and film formation seem to have an impact on the molecular mobility of hydrogen in the polymer particles. It seems that drying causes a decrease in T_1 because of an increase in molecular mobility,

https://dx.doi.org/10.1021/acsomega.0c06010
ACS Omega 2021, 6, 7499−7511

and film formation causes an increase in T_1 time because of the loss of molecular mobility. During the hydration of a polymer−cement composite at room temperature, both effects (drying and film formation) can take place synchronously if a soft polymer is used, which is caused by the consumption of water in the hydration process.

The big difference in such experiments is due to the polymer used. If a soft polymer is used that forms films at room temperature, both effects can be assumed. The T_1 time shift results from drying and film formation, and hence the shift in T_1 has to be less than that for a hard polymer that only loses water without film formation. The reason for this assumption is based on the fact that the T_1 time shifts because of drying and film formation are opposite, as shown above.

Figure 13 finally shows the T_1 time evolution of hydrogen in the polymer particles during the hydration of a cement−polymer composite (10 wt % polymer) at 23 °C with two different polymers.

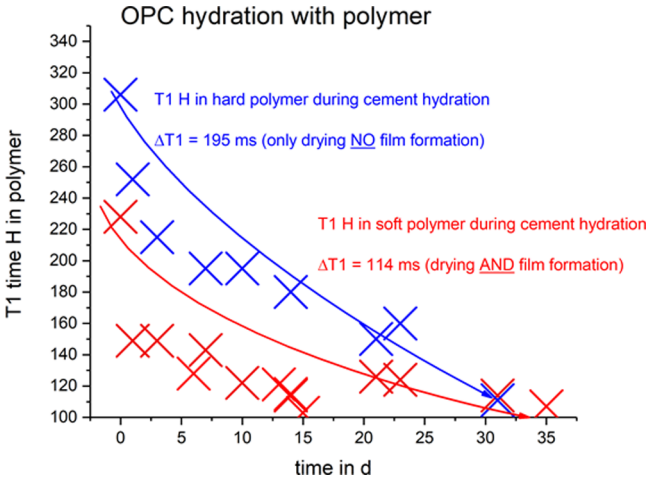

Figure 13. T_1 time shift of hydrogen in the polymer particles during the hydration of a cement−polymer composite (10 wt % polymer); 23 °C. Comparison of a hard polymer and a soft polymer.

It can be seen that the hard polymer shows a T_1 time shift of 195 ms, whereas the soft polymer shows a T_1 time shift of 114 ms. It is most likely that the delta in T_1 time gives an idea of the film formation.

If the polymer particles do not form films, only the drying of the polymer particles mainly contributes to the T_1 time shift, leading to a quite high T_1 time shift. If the drying is accompanied by a film formation process, the T_1 time shift is a combination of drying and film formation. It can be assumed that the shift in T_1 time is less because both effects act oppositely with regard to the T_1 time, and only the T_1 time shift as a sum of both processes (drying and film formation) can be detected.

However, this is an initial interpretation and has to be proven in detail further. The T_1 time shift during drying/film formation is also a function of the polymer composition. In order to prove this impact, further studies will be performed using special synthesized polymers. The results from these experiments will be published in the future.

CONCLUSIONS

In the last decades, large efforts have been paid to link the processes within a combined organic and inorganic system to the final performance of the resulting hybrid system. Because of the lack of suitable nondestructive analytical methods, the simultaneous monitoring of the latex film formation and the hydration of cement (consumption of water) is still an issue. Therefore, our motivation was to find a novel analytical method.

The following conclusions can be drawn from the presented data: a method is presented that gives an idea of the suitability of an affordable, artifact-free benchtop method for synchronously tracking cement hydration and film formation. Compared to other methods such as (cryo)-SEM and TEM, it has the advantage that a nondestructive bulk analysis can be performed that provides signals free of artifacts.

As shown, a special approach with ^{1}H-TD-NMR, namely the T_2 time-weighted T_1 time evaluation, is very promising for the deconvolution of all the hydrogen reservoirs in the sample. In comparison to T_2 time, the reservoirs for the highly confined hydrogen, namely ettringite, portlandite, AFm, and polymer, can be separated from the intermediate bound hydrogen in the C−S−H phase and free water. A further separation can be done using T_1 time, and an isolated signal for hydrogen bound in the polymer particle can be obtained.

The T_1 time shift of the polymer during the hardening of a cement−polymer−composite with water seems to be driven first by the drying of the polymer particles and second by the interdiffusion of the polymer chains causing a homogeneous film. Further studies must be carried out in order to understand the impact of the polymer composition on the T_1 time shift during film formation.

On the basis of the performed experiments, it must be concluded that the film formation of the polymer particles during the hydration of a cement (OPC), applying a w/c ratio of 0.5, is a process that takes place over days instead of within the first few hours.

As an outlook, this method might allow us to link the temporal order of film formation and hydration to the final properties of the construction material, such as the mechanical properties (elongation at break, tensile strength, and adhesion), the sealing properties (waterproofing), the durability, and how fast the processing/drying time can be.

AUTHOR INFORMATION

Corresponding Authors

Daniel Jansen − *Mineralogy, GeoZentrum Nordbayern, 91054 Erlangen, Germany*; orcid.org/0000-0003-2302-9386; Phone: +49 9131 85 25844; Email: Daniel.Jansen@fau.de

Xiangming Kong − *Department of Civil Engineering, Tsinghua University, 100084 Beijing, China*; Phone: +86-10-62783703; Email: kxm@mail.tsinghua.edu.cn

Authors

Dominique Ectors − *Mineralogy, GeoZentrum Nordbayern, 91054 Erlangen, Germany*

Christian Schmidtke − *BASF Construction Additives, 83308 Trostberg, Germany*

Florian Deschner − *BASF Construction Additives, 83308 Trostberg, Germany*

Joachim Pakusch − *BASF SE, 67056 Ludwigshafen am Rhein, Germany*

Ekkehard Jahns − *BASF SE, 67056 Ludwigshafen am Rhein, Germany*

Jürgen Neubauer − *Mineralogy, GeoZentrum Nordbayern, 91054 Erlangen, Germany*

https://dx.doi.org/10.1021/acsomega.0c06010
ACS Omega 2021, 6, 7499−7511

Complete contact information is available at:
https://pubs.acs.org/10.1021/acsomega.0c06010

Notes

The authors declare no competing financial interest.

■ ACKNOWLEDGMENTS

The authors would like to thank Dr. Markus Rückel (BASF SE) for his support and helpful discussions.

■ REFERENCES

(1) Ohama, Y. *Handbook of Polymer-Modified Concrete and Mortars*; Noyes Publications: Park Ridge, New Jersey, 1995.
(2) Sakai, E.; Sugita, J. Composite mechanism of polymer modified cement. *Cem. Concr. Res.* **1995**, *25*, 127−135.
(3) De Vekey, R. C.; Majumdar, A. J. Durability of cement pastes modified by polymer dispersions. *Mater. Struct.* **1975**, *8*, 315−321.
(4) Chevalier, Y.; Pichot, C.; Graillat, C.; Joanicot, M.; Wong, K.; Maquet, J.; Lindner, P.; Cabane, B. Film formation with latex particles. *Colloid Polym. Sci.* **1992**, *270*, 806−821.
(5) Keddie, J. L.; Routh, A. F. *Fundamentals of Latex Film Formation*; Springer, 2010.
(6) Chen, X.; Fischer, S.; Yi, Z.; Boyko, V.; Terrenoire, A.; Reinhold, F.; Rieger, J.; Li, X.; Men, Y. Structural Reorganization of a Polymeric Latex Film During Dry Sintering at Elevated Temperatures. *Langmuir* **2011**, *27*, 8458−8463.
(7) Rottstegge, J.; Traub, B.; Wilhelm, M.; Landfester, K.; Heldmann, C.; Spiess, H. W. Investigations on the film-formation process of latex dispersions by solid-state NMR Spectroscopy. *Macromol. Chem. Phys.* **2003**, *204*, 787−802.
(8) Ludwig, I.; Schabel, W.; Kind, M.; Castaing, J.-C.; Ferlin, P. Drying and film formation of industrial waterborne lattices. *AIChE J.* **2007**, *53*, 549−560.
(9) Baueregger, S.; Perello, M.; Plank, J. Influence of anti-caking agent kaolin on film formation of ethylene-vinylacetate and carboxylated styrene-butadiene latex polymers. *Cem. Concr. Res.* **2014**, *58*, 112−120.
(10) Besghini, D.; Mauri, M.; Simonutti, R. Time Domain NMR in polymer science: From the laboratory to the industry. *Appl. Sci.* **2019**, *9*, 1801.
(11) Voogt, B.; Huinink, H. P.; Erich, S. J. F.; Scheerder, J.; Venema, P.; Keddie, J. L.; Adan, O. C. G. Film formation of high Tg latex using hydroplasticization: Explanations from NMR Relaxometry. *Langmuir* **2019**, *35*, 12418−12427.
(12) Lothenbach, B.; Winnefeld, F. Thermodynamic modelling of the hydration of Portland cement. *Cem. Concr. Res.* **2006**, *36*, 209−226.
(13) Scrivener, K. L.; Nonat, A. Hydration of cementitious materials, present and future. *Cem. Concr. Res.* **2011**, *41*, 651−665.
(14) Jansen, D.; Goetz-Neunhoeffer, F.; Lothenbach, B.; Neubauer, J. The early hydration of Ordinary Portland Cement (OPC): An approach comparing measured heat flow with calculated heat flow from QXRD. *Cem. Concr. Res.* **2012**, *42*, 134−138.
(15) Jansen, D.; Goetz-Neunhoeffer, F.; Stabler, C.; Neubauer, J. A remastered external standard method applied to the quantification of early OPC hydration. *Cem. Concr. Res.* **2011**, *41*, 602−608.
(16) Taylor, H. F. W. *Cement Chemistry*; Thomas Telford Publishing, 1990.
(17) McDonald, P. J.; Gajewicz, A. M. *The Characterization of Cement Based Materials Using T_2 ^1H Nuclear Magnetic Resonance Relaxation Analysis. Good Practice Guide No. 144*; National Physical Laboratory UK, 2016.
(18) Muller, A. C. A.; Scrivener, K. L.; Gajewicz, A. M.; McDonald, P. J. Use of bench-top NMR to measure the density, composition and desorption isotherm of C-S-H in cement paste. *Microporous Mesoporous Mater.* **2013**, *178*, 99−103.
(19) Muller, A. C. A.; Scrivener, K. L.; Gajewicz, A. M.; McDonald, P. J. Densification of C-S-H measured by 1H NMR Relaxometry. *J. Phys. Chem. C* **2013**, *117*, 403−412.
(20) Jansen, D.; Naber, C.; Ectors, D.; Lu, Z.; Kong, X.-M.; Goetz-Neunhoeffer, F.; Neubauer, J. The early hydration of OPC investigated by in-situ XRD, heat flow calorimetry, pore water analysis and 1H NMR: Learning about adsorbed ions from a complete mass balance approach. *Cem. Concr. Res.* **2018**, *109*, 230−242.
(21) Jansen, D.; Wolf, J. J.; Fobbe, N. The hydration of nearly pure ye'elimite with a sulfate carrier in a stoichiometric ettringite binder system: Implications for the hydration process based on in-situ XRD, 1-H-TD-NMR, pore solution analysis and thermodynamic modelling. *Cem. Concr. Res.* **2020**, *127*, 105923.
(22) Ectors, D.; Goetz-Neunhoeffer, F.; Hergeth, W.-D.; Dietrich, U.; Neubauer, J. In situ 1H-TD-NMR: Quantification and microstructure development during the early hydration of alite and OPC. *Cem. Concr. Res.* **2016**, *79*, 366−372.
(23) Muller, A. C. A.; Scrivener, K. L. A reassessment of mercury intrusion porosimetry by comparison with 1H NMR relaxometry. *Cem. Concr. Res.* **2017**, *100*, 350−360.
(24) McDonald, P. J.; Rodin, V.; Valori, A. Characterisation of intra- and inter-C-S-H gel pore water in white cement based on an analysis of NMR signal amplitudes as a function of water content. *Cem. Concr. Res.* **2010**, *40*, 1656−1663.
(25) Naber, C.; Kleiner, F.; Becker, F.; Nguyen-Tuan, L.; Rößler, C.; Etzold, M. A.; Neubauer, J. C-S-H Pore Size Characterization Via a Combined Nuclear Magnetic Resonance (NMR)-Scanning Electron Microscopy (SEM) Surface Relaxivity Calibration. *Materials* **2020**, *13*, 1779.
(26) Jansen, D.; Lu, Z.; Kong, X.-M.; Pakusch, J.; Jahns, E.; Deschner, F.; Schmidtke, C. The influence of the glass transition temperature of polymers on early OPC hydration: A complete study of the heat flow, phase evolution, and pore solution chemistry. *Mater. Struct.* **2019**, *52*, 120.
(27) Lu, Z.; Kong, X.; Zhang, C.; Jansen, D.; Neubauer, J.; Goetz-Neunhoeffer, F. Effects of two oppositely charged colloidal polymers on cement hydration. *Cem. Concr. Compos.* **2019**, *96*, 66−76.
(28) Kong, X.; Pakusch, J.; Jansen, D.; Emmerling, S.; Neubauer, J.; Goetz-Neuhoeffer, F. Effect of polymer latexes with cleaned serum on the phase development of hydrating cement pastes. *Cem. Concr. Res.* **2016**, *84*, 30−40.
(29) Jansen, D.; Goetz-Neunhoeffer, F.; Neubauer, J.; Hergeth, W. D.; Haerzschel, R. Influence of polyvinyl alcohol on phase. *ZKG Int.* **2010**, *63*, 100−107.
(30) Rietveld, H. M. The Rietveld Method. *Phys. Scr.* **2014**, *89*, 098002.
(31) O'Connor, B. H.; Raven, M. D. Application of the Rietveld refinement procedure in assaying powdered mixtures. *Powder Diffr.* **1988**, *3*, 2−6.
(32) Jansen, D.; Stabler, C.; Goetz-Neunhoeffer, F.; Dittrich, S.; Neubauer, J. Does Ordinary Portland Cement contain amorphous phase? A quantitative study using an external standard method. *Powder Diffr.* **2011**, *26*, 31−38.
(33) Schreiner, J.; Jansen, D.; Ectors, D.; Goetz-Neunhoeffer, F.; Neubauer, J.; Volkmann, S. New analytical possibilities for monitoring the phase development during the production of autoclaved aerated concrete. *Cem. Concr. Res.* **2018**, *107*, 247−252.
(34) Powles, J. G.; Strange, J. H. Zero Time Resolution Nuclear Magnetic Resonance Transient in Solids. *Proc. Phys. Soc.* **1963**, *82*, 6.
(35) Naber, C.; Bellmann, F.; Sowoidnich, T.; Goetz-Neunhoeffer, F.; Neubauer, J. Alite dissolution and C-S-H precipitation rates during hydration. *Cem. Concr. Res.* **2019**, *115*, 283−293.
(36) Scrivener, K.; Ouzia, A.; Juilland, P.; Kunhi Mohamed, A. Advances in understanding cement hydration mechanisms. *Cem. Concr. Res.* **2019**, *124*, 105823.
(37) Carr, H. Y.; Purcell, E. M. Effects of diffusion on free precession in nuclear magnetic resonance experiments. *Phys. Rev.* **1954**, *94*, 630−638.

https://dx.doi.org/10.1021/acsomega.0c06010
ACS Omega 2021, 6, 7499−7511

(38) Meiboom, S.; Gill, D. Modified spin-echo method for measuring nuclear relaxation times. *Rev. Sci. Instrum.* **1958**, *29*, 688−691.
(39) Provencher, S. W. A constrained regularization method for inverting data represented by linear algebraic or integral equations. *Comput. Phys. Commun.* **1982**, *27*, 213−227.
(40) Holthausen, R. S.; Raupach, M. A phenomenological approach on the influence of paramagnetic iron in cement stone on 2D T1-T2 relaxation in single-sided 1H nuclear magnetic resonance. *Cem. Concr. Res.* **2019**, *120*, 279−293.
(41) Muller, A.; Mitchell, J.; McDonald, P. J. Proton nuclear magnetic resonance relaxometry. *A Practical Guide to Microstructural Analysis of Cementitious Materials*; CRC Press, Taylor & Francis Group, 2016.
(42) Valori, A.; McDonald, P. J.; Scrivener, K. L. The morphology of C-S-H: Lessons from ^{1}H nuclear magnetic resonance relaxometry. *Cem. Concr. Res.* **2013**, *49*, 65−81.

https://dx.doi.org/10.1021/acsomega.0c06010
ACS Omega 2021, 6, 7499−7511